A Census of Precipitation Features in the Tropics Using TRMM: Radar, Ice Scattering, and Lightning Observations

Stephen W. Nesbitt and Edward J. Zipser

Department of Meteorology, University of Utah, Salt Lake City, Utah

Daniel J. Cecil

Department of Atmospheric Sciences, Texas A&M University, College Station, Texas

ABSTRACT

An algorithm has been developed to identify precipitation features ($\geq$75 km^2 in size) in two land and two ocean regions during August, September, and October 1998. It uses data from two instruments on the Tropical Rainfall Measuring Mission (TRMM) satellite: near-surface precipitation radar (PR) reflectivities, and TRMM Microwave Imager (TMI) 85.5-GHz polarization corrected temperatures (PCTs). These features were classified by size and intensity criteria to identify mesoscale convective systems (MCSs), precipitation with PCTs below 250 K, and other features without PCTs below 250 K. By using this technique, several hypotheses about the convective intensity and rainfall distributions of tropical precipitation systems can be evaluated. It was shown that features over land were much more intense than similar oceanic features as measured by their minimum PCTs, maximum heights of the 30-dBZ contour, and 6-km reflectivities. The diurnal cycle of precipitation features showed a strong afternoon maximum over land and a rather flat distribution over the ocean, quite similar to those found by others using infrared satellite techniques. Precipitation features with MCSs over the ocean contained significantly more rain outside the 250-K PCT isotherm than land systems, and in general, a significant portion (10%–15%) of rainfall in the Tropics falls in systems containing no PCTs less than 250 K. Volumetric rainfall and lightning characteristics (as observed by the Lightning Imaging Sensor aboard TRMM) from the systems were classified by feature intensity; similar rain amounts but highly differing lightning flash rates were found among the regions. Oceanic storms have a bimodal contribution of rainfall from two types of systems: very weak systems with little ice scattering and moderately strong systems that do not produce high lightning flash rates. Continental systems that produce the bulk of the rainfall (as sampled) are likely to have higher lightning flash rates, which are shown to be linked to stronger radar and ice-scattering intensities.

1. Introduction

The classification of precipitation features often grew out of the instruments used to observe and quantify them. Maddox (1980) defined the mesoscale convective complex (MCC) using infrared satellite brightness temperature thresholds of size, duration, and shape; however, cloud-top temperatures are not very well related to the physical processes within storms, and thus, the rainfall contained in the system. These systems, despite being responsible for less than 1% of total cloud clusters by size (Mapes and Houze 1993), contribute much more significantly to the rainfall in regions where they are observed. However, infrared measurement of these systems may not be the best tool to determine the radiation

budgets and rainfall produced by these systems. In contrast, Houze (1993) defines a mesoscale convective system (MCS) "as a cloud system that occurs in connection with an ensemble of thunderstorms and produces a contiguous precipitation area ∼100 km or more in horizontal scale in at least one direction." Here the definition is constrained by the size and intensity of the precipitation created within it. Convective intensity and/or rainfall measurement is a means of distinguishing the distribution of systems that produce the bulk of the heat, momentum, and moisture fluxes in the Tropics and subtropics (i.e., quantifying the "hot towers," Riehl and Malkus 1958).

Large-scale rainfall measurement with ground- or aircraft-based radars or gauge data is not feasible, but passive microwave satellite techniques do allow a larger-scale quantification of convective processes. At microwave frequencies greater than 30 GHz, ice hydrometeors primarily scatter radiation upwelling from the surface. This results in a depression of brightness temperatures

Corresponding author address: Stephen W. Nesbitt, Department of Meteorology, University of Utah, 135 South 1460 East Room 819, Salt Lake City, UT 84112-0110.
E-mail: snesbitt@met.utah.edu

in areas where significant optical depths of ice hydrometeors are present (Spencer 1986); at 85-GHz emission from rain is minimized, leaving signatures from ice hydrometeors. The use of polarization corrected temperature (PCT; Spencer et al. 1989) allows the removal of surface polarization effects, leading to PCT being an unambiguous precipitation-sized ice particle quantifier. Mohr and Zipser (1996, hereafter MZ) used the 85-GHz PCT from the Special Sensor Microwave Imager (SSM/I) to obtain a sample of MCSs (noting their location, size, and intensity) as defined by their ice scattering signatures. They defined the *ice scattering MCS* as a contiguous area greater than 2000 km^2 with PCT less than 250 K with at least one data bin with a PCT of 225 K or less (to ensure convection in the system). Because the ice scattering signature ($\leq$250 K) of a system is almost always smaller than the precipitation area, the MZ (1996) criteria are roughly analogous to the Houze (1993) MCS definition. Using these criteria, a climatology was created for four months of observed MCSs throughout the Tropics from 1993.

Despite the creation of a large sample of undoubtedly precipitating systems, MZ's analysis of their MCSs did not allow an accurate quantification of MCSs role in the tropical precipitation budget. Ice scattering signature at 85 GHz, notwithstanding its correlation to relative ice particle size, optical depth, and concentration, does not relate as directly to surface rainfall as other measurements. Significant precipitation may also occur at 85 PCTs greater than 250 K, especially at the coarse resolution of the SSM/I (13 $\times$ 15 km^2 at 85 GHz). So, this approach certainly introduces sensitivity issues in estimating the properties of ice scattering MCSs.

Mohr et al. (1999) furthered their previous work with the SSM/I by quantifying the contribution of rainfall from ice scattering MCSs versus other ice scattering precipitation systems. Systems with PCT $\leq$250 K were subdivided into four classes, ranging from the large MZ (1996) MCS to smaller systems containing only one 13 $\times$ 15 km^2 SSM/I data bin $\leq$250 K. The rainfall was estimated from these systems using the GSCAT algorithm where brightness temperatures were related to a rain rate. Using the ice scattering method (which is not as direct a rain measurement as a radar estimation, for example), it was found that while MCSs contributed only 10%–20% of the sampled systems by number, they contributed 70%–80% of the rainfall throughout the Tropics. Also, the oceanic regions' precipitation systems that contributed the most toward the total rainfall contained minimum PCTs closely centered at 200 K, while the land regions had a broader distribution of minimum PCTs centered between 150 and 175 K. An exception to this is the Amazon region. Despite being a large land region, it had rainfall characteristics similar to those over the ocean.

As before, the employment of an ice scattering precipitation algorithm introduces significant uncertainties in rainfall estimation and contribution to total rainfall for large and small systems alike. For small systems, using the SSM/I resolution raises serious beamfilling issues. In general, the occurrence of precipitation features without an ice scattering signature (i.e., warm rain or light rain) is often observed in the Tropics and is not able to be quantified using an ice scattering technique alone. One of the goals of this study is to evaluate the extent of this particular shortcoming of ice scattering rainfall estimation techniques.

To better estimate the tropical rainfall budget, a more direct and sensitive rainfall estimation technique is necessary. Rickenbach and Rutledge (1998) used Tropical Ocean and Global Atmosphere Coupled Ocean–Atmosphere Response Experiment (TOGA COARE) ground-based radar data to classify precipitating systems by type and estimate their rainfall contribution. Using spaceborne radar [the precipitation radar (PR)] will allow the use of this direct rainfall estimation technique throughout the Tropics, without being restricted to the fixed locations of ground-based radars.

In spite of difficulties with rainfall estimation in the Tropics, issues of land versus ocean convective intensity have been somewhat better understood. Lightning flash rates can be a surrogate for the convective intensity of the lightning-producing storm. The magnitude of charge separation leading to cloud electrification is likely due to the occurrence of ice particle collisions in the presence of supercooled water in the mixed phase region (between 0° and −40°C, Williams et al. 1991). Laboratory (e.g., Takahashi 1978) and field (e.g., Dye et al. 1986) measurements have corroborated this. Observations of storms have shown a disparity between the lightning flash rates of continental versus oceanic convection theorized to be linked to the difference in mean updraft speeds between the two areas (Jorgensen and LeMone 1989; Lucas et al. 1994; Zipser and Lutz 1994). Lightning over the ocean is thought to be uncommon because the updrafts are too weak to loft sufficient amounts of large particles into the mixed phase region of the cloud (Williams et al. 1992; Zipser and Lutz 1994). Field program data suggest that the strongest 10% of updrafts over the ocean are less than half as strong as severe storm updrafts observed in a continental regime (Lucas et al. 1994; Zipser and LeMone 1980; Jorgensen et al. 1985; Jorgensen and LeMone 1989). The lack of ice aloft is reflected in observations of 85-GHz PCT, since PCT is correlated to the optical depth of ice in the field of view of the radiometer. Both MZ (1996) and Mohr et al. (1999) estimated the intensity of precipitation features using their algorithms and found distinctly lower minimum PCTs in convective cores in land versus ocean MCSs. The availability of large-scale radar measurements over the Tropics would allow the 3D quantification of these intensity differences.

The larger questions of tropical convective intensity and rainfall may be addressed with the coincident remote sensing observations of the Tropical Rainfall Measuring Mission (TRMM) satellite. By utilizing the PR

to quantify the three-dimensional structure of tropical precipitation, we can answer the following questions.

- What are the intensity[1] differences between precipitation features of various spatial scales in specific tropical regions? The PR is used to compare reflectivity characteristics of systems (from small features to MCSs) over land and ocean, and regionally throughout the Tropics. For these same systems, the TRMM Microwave Imager (TMI) is used to assess the intensity of ice scattering. By using similar definitions of ice scattering MCSs as in MZ and Mohr et al. (1999), previous work can be related to observations using the improved resolution of the TMI, and in addition compared with the PR's statistics on the vertical extent of strong radar echoes.

- What is the contribution of various precipitation feature classes to the total population of features and total rainfall in the various regions of the Tropics? The PR has many advantages in the detection and estimation of rainfall contribution over microwave techniques: 1) detection of near-surface rainfall by radar yields a much more direct estimate of precipitation than by ice scattering techniques, 2) higher resolution (by a factor of 10 over the SSM/I) tempers the beamfilling problems previously suffered, 3) sampling throughout the diurnal cycle allows better quantification of rainfall than the sunrise/sunset orbital pattern of the SSM/I, and 4) using radar for the measurement of precipitation allows the detection of rain occurring at $T_B > 250$ K that is unable to be measured using previous ice scattering techniques. Precipitation missed by ice scattering techniques may include light rainfall, and heavy rainfall that may be occurring either on small scales or without significant ice scattering signatures (''warm rain''). In this way we can evaluate some of the shortcomings in the previous use of ice scattering precipitation techniques. Potentially this kind of validation of ice scattering precipitation estimation techniques can improve rainfall estimates

from more than 10 years of SSM/I data that has been collected.

- What are lightning frequency differences for the types of precipitation features as identified by the PR and TMI? The Lightning Imaging Sensor (LIS) instrument can measure flash rate differences among the precipitation features observed. Differences in observed flash rate over the different tropical regions can then be compared with the PR and TMI intensity characteristics.

This study will use an algorithm that identifies and classifies individual precipitation features using TRMM's PR and TMI. The characteristics of the identified features will then be used to address the above questions.

2. Data and methods

a. Satellite and instrumentation

The TRMM satellite was launched in 1997 and has been providing nearly continuous observations of tropical precipitation (between 35°N and 35°S) since its launch date. It orbits at an altitude of approximately 350 km. Due to the orbit not being sun-synchronous, the full diurnal cycle can be sampled by TRMM with a sufficiently large sample of orbits (as opposed to the sunrise/sunset passes of the SSM/I). It takes about 47 days for the instruments to sample the complete cycle. This study employs 92 days of data to avoid biases introduced by incomplete diurnal sampling. Kummerow et al. (1998) provides complete specifications of the PR and TMI instruments, while Christian (1999) details the LIS instrument.

The PR is the first quantitative spaceborne radar. The PR was developed by the Japanese space agency (the National Space Development Agency) and the Communications Research Laboratory in Tokyo, Japan. It utilizes a 2-m phased-array antenna that provides a horizontal resolution of 4.3 × 4.3 km² at nadir. With a minimum detectable signal of approximately 15 dBZ, the PR can reliably detect precipitation despite its low-transmission power ($\sim$500 W). It has a 215-km swath width that extends 20 km above the earth ellipsoid with a 250-m vertical resolution. It has a frequency near 13.8 GHz, which means that the beam is subject to attenuation in heavy precipitation areas. This study utilizes the 2A-25 version 4.0 algorithm[2] reflectivity profiles that correct for attenuation using two methods. A surface reference method, used most often in moderate to heavy precipitation, utilizes the decrease in the intensity of the surface ground clutter to estimate total path attenuation. Mainly in light precipitation, this first method is aided

---

[1] Intensity is used here in a general qualitative sense to refer to the updraft magnitudes associated with a particular convective system. We believe that such use is at least as plausible as the more common association of intense convection with high-reflectivity cores or very cold cloud tops.

Aircraft remote sensing observations (e.g., Hakkarinen and Adler 1988; Heymsfield et al. 1996) have shown that large densities of scatterers above the freezing level (i.e., high radar reflectivities aloft) scatter a large portion of the upwelling 85-GHz radiation out of the field of view of the radiometer, thus lowering PCTs. Radiative transfer (Vivekanandan et al. 1991) and dynamical modeling studies (Smith et al. 1992; Mugnai et al. 1993) have also shown a direct relationship between low brightness temperatures in frequencies near 85 GHz and large optical depths of high-density ice particles (graupel as parameterized in Smith et al.). These large optical depths of graupel aloft must originate, in large part, from strong updrafts with high supercooled water content with the ability to grow ice particles by riming and loft them well above their formation zone. Thus, intense ice scattering and intense radar echo aloft both imply intense convection.

[2] Specifications of the 2A-25 algorithm may be found on the World Wide Web at http://tsdis02.nascom.nasa.gov/tsdis/Documents/ICSVol4.pdf.

by a modified Hitchfield–Borden attenuation correction scheme that uses the reflectivity profile itself to estimate attenuation (Iguchi and Meneghini 1994). Both these methods are used to avoid the calculation of a divergent reflectivity solution. Also, the 2A-25 algorithm removes the surface ground clutter to leave an attenuation-corrected reflectivity profile of precipitation.

The TMI similar in many respects to the SSM/I instrument orbiting the earth since the mid-1980s. However, because of TRMM's lower altitude orbit, the TMI achieves higher resolution than the SSM/I. It is a conically scanning passive microwave radiometer with a 759-km swath width. At 85.5 GHz, the TMI has an effective field of view of 4×7 km^2 in the across-track and down-track directions, respectively. This investigation uses the ice scattering signature of precipitation at 85.5 GHz. At this frequency, there is some lowering in PCT from cloud water effects (by about 10°), but the volume scattering by precipitation (large ice particles) will result in decreases in brightness temperature below 275 K. With the surface appearing warm at these frequencies, ice particles scatter radiation out of the satellite's field of view (FOV) as well as reflect the cold cosmic background radiation (with a brightness temperature = 2.7 K) into the satellite's FOV.

At these high frequencies, the ocean's emissivity is a strong function of polarization at oblique viewing angles like the TMI's. In addition, nonuniform surface characteristics over land cause emissivity differences. Because of this, the horizontally and vertically polarized background brightness temperatures greatly differ depending on surface emissivities, which causes discontinuities (especially at coastlines). Spencer et al.(1989) developed the PCT that largely removes these ambiguities. This parameter is calculated by the following (from Spencer et al. 1989):

$$\text{PCT} = \frac{\beta T_{B_h} - T_{B_v}}{\beta - 1}.$$

The parameter β was derived to be 0.45 to yield background PCTs between 275 and 290 K. PCTs depressed below 250 K are likely precipitation and not contamination from a cold ocean background. Surface snow cover may lead to false precipitation retrievals, and a technique will be defined below to remove these artifacts. With all artifacts removed, examining distributions of 85-GHz ice scattering of precipitation features in the Tropics gives insight into the microphysical characteristics of the systems observed.

The LIS instrument is a staring optical imager that identifies changes in radiance in the FOV that it observes. Using the oxygen emission line at 777.4 nm, LIS achieves a 3–6-km resolution (3 km at nadir). The detector attains a 90% viewing efficiency of the lightning "flashes" it observes (Christian 1999). It has roughly a 600×600 km^2 viewing area, which is oriented parallel to the satellite track to allow roughly equal

viewing time (~90 s) of all areas in the swath. This "viewtime" is useful for calculating flash rates at a particular location. However, this work simply presents observations of flashes to relate relative lightning frequencies to storm type. This method allows detection of total lightning; both in-cloud and cloud-to-ground lightning flashes are measured. Because of lightning–updraft strength hypotheses (e.g., Williams et al. 1992; Zipser and Lutz 1994; and others), lightning flash information can be used as a proxy for convective vigor in comparing storms' intensities.

b. Experimental design

In order to identify discrete precipitation features in the Tropics, data from the PR 2A-25 near-surface reflectivity product is used in combination with the TMI 85-GHz PCT. Three months of TRMM data from August, September, and October 1998 have been selected for analysis in this study. Four regions have been selected to compare: Africa, South America, east Pacific, and west Pacific. (The boundaries of these areas appear in the results in Fig. 3.) These regions were selected to enable the sampling of precipitation features in climatologically rainy areas in the deep Tropics in or near the ITCZ. The features contained within them consist of a large, archetypical sample of continental and oceanic precipitation systems. This analysis also allow the comparison between the four regions to examine differences in all regions' precipitation features.

The selection of observational criteria to identify precipitation features was conducted with several goals in mind. A complete sampling of precipitation was desired, reaching from the individual convective shower to the large MCC. However, the PR's relatively coarse resolution compared to the scale of individual cumulonimbus clouds does not allow the sampling of the very small features. Also, low-altitude random noise near the minimum detectable signal of the PR inhibits the selection of individual data bins as precipitation features. (Note that a data bin corresponds to an area of 18.5 km^2 corresponding to the horizontal area of a PR FOV at the surface.) Inclusion of this noise would bias any statistics of the storms sampled. For this reason, a minimum precipitation feature size of four data bins has been chosen to remove noise from the dataset, albeit arbitrarily. This corresponds to an area of approximately 75 km^2.

To sample all precipitation and the surrounding deeper cloud systems, both the ice scattering signature and low-level radar signature are used to select precipitation features. As mentioned previously, these two TRMM instruments have different scan strategies that inhibit direct matching of the raw data. So, an interpolation scheme is required to match the retrievals. In this study, a "nearest neighbor" interpolation is used with the PR data bin locations (on a quasi-regularly spaced 4.3×4.3 km^2 grid) used as a basis for the interpolation. Within the PR swath only, *TMI brightness temperatures are*

collocated with the closest PR data bin locations. Because the TMI resolution at this frequency places data bins roughly every 14 km in the along-track direction, typically two or three PR data bins are assigned the same TMI brightness temperature. This nearest neighbor collocation was done to ensure inclusion of the extrema in brightness temperatures so crucial in the determination of relative ice concentration.

Once the two fields are matched, then a selection of the precipitation features ($\geq$4 data bins in size) was performed. These are systems with contiguous data bins touching (i.e., edges or corners adjacent). All areas with near-surface reflectivity $\geq$20 dB*Z* or PCT $\leq$250 K were selected to ensure each system contained both the low-level precipitation field and associated areas of ice scattering aloft (i.e., anvils). This was motivated by the desire to sample the entire extent of the system, which often extends beyond either the surface rain or ice scattering signatures alone. Snow cover in high-elevation regions of the Tropics (e.g., the Andes Mountains) may artificially depress PCTs outside areas of real precipitation (due to the snow's low emissivity compared with snow-free land areas). Maintaining that the maximum near-surface reflectivity or 6-km reflectivity in a precipitation feature be greater than 15 dBZ (close to the minimum detectable signal of the PR) in a feature with a data bin with PCT $\leq$250 K ensures that these spurious snow features were removed. This is justified as it is very unlikely that precipitation is occurring (with a PCT <250) without some appreciable radar echo at either of these two levels >15 dBZ.

Once these systems have been selected and snow artifacts have been removed, they were classified by the size and intensity criteria appearing below.

c. Description of the precipitation feature classifications

Figure 1 presents a schematic of the three types of precipitation feature classifications based on their near-surface reflectivity and PCT characteristics. The specific criteria used for identification of the systems using the *dual*-instrument method appear in Table 1a. In addition, this study used the PCT characteristics of the precipitation features to compare with the MCSs and intense MCSs identified by MZ (1996). Hereafter, these features identified by their ice scattering signature will be referred to as MZ equivalent features; the criteria used for their identification appear in Table 1b. However, the following is a description of each of the precipitation features identified using the their near-surface reflectivity and PCT characteristics.

1) PRECIPITATION FEATURE WITHOUT ICE SCATTERING

The precipitation feature without ice scattering category includes systems containing surface precipitation without an associated ice scattering signature (with PCT $\leq$250 K). This is not to say that there are no ice processes occurring in the system, simply that they were either too weak or too small to be detected at the TMI resolution. This type of feature was chosen in order to identify warm rain and weak and/or decaying convection.

2) PRECIPITATION FEATURE WITH ICE SCATTERING

The precipitation feature with ice scattering category includes features that do not meet MCS criteria, but include at least one data bin with PCT $\leq$250 K. This ensures that there is significant ice scattering occurring, meaning that significant optical depths of precipitation-sized ice particles (more likely graupel than snow as modeled by Vivekanandan et al. 1991; Smith et al. 1992; Mugnai et al. 1993) are present in the feature. This category identifies precipitation features ranging in size from small precipitation features 75 km^2 in size to large systems not meeting the MCS area or intensity criteria, as defined in the next section.

3) PRECIPITATION FEATURE WITH AN MCS

The precipitation feature with an MCS category is based upon the classification of MZ (1996), who sampled the properties of ice scattering MCSs using the SSM/I instrument. This work seeks to match MZ's ice scattering MCS definition. This category requires 108 contiguous data bins (area ~2000 km^2) with PCT $\leq$250 K to be contained within the rain or ice scattering area of the system. In addition, 10 noncontiguous data bins (area ~185 km^2) within the 2000-km^2 area must contain PCT $\leq$225 K to ensure the presence of a large optical depth of ice and thus a deep convective layer within the storm. Note that the precipitation feature with an MCS category may contain more than one area meeting the MZ equivalent PCT criteria below, *and* the rain falling at PCTs $\geq$250 K contiguous with the depressed ice scattering area.

4) MZ EQUIVALENT MCSs

As a sensitivity test, a comparison was performed comparing MCSs analyzed with their ice scattering *and* rainfall characteristics (the precipitation feature with an MCS category defined above) and those defined by the TMI ice scattering signature alone as done by MZ (1996). By performing such a comparison, it is possible to compare the combined TMI and PR estimate of rainfall and other physical characteristics with those estimated by the TMI alone. The features identified by their PCT characteristics are called *MZ equivalent MCS* and *MZ equivalent intense MCS* because of their similarity with those features identified by MZ. The criteria for selection of these features appears in Table 1b. It is important to note that the identification of the MZ equiv-
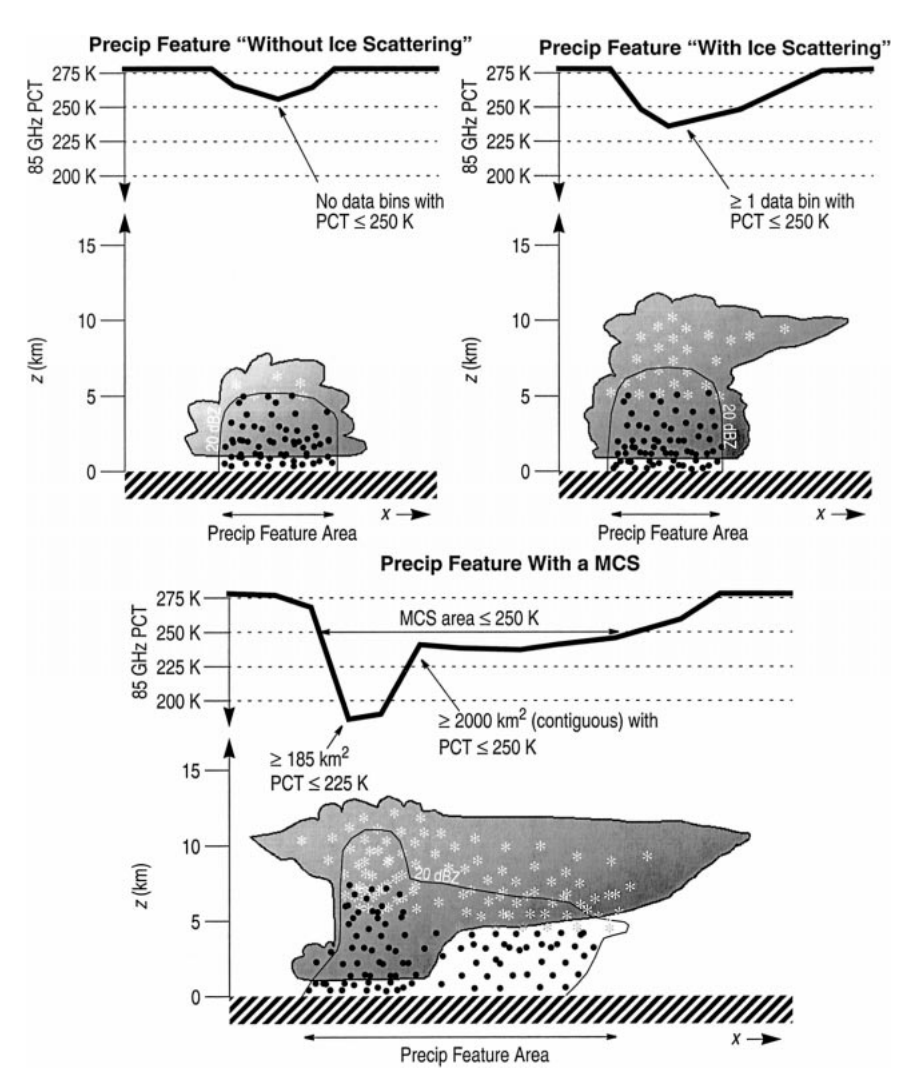
FIG. 1. Vertical cross-section schematic of the three precipitation feature types. Above each example cloud (ice and liquid hydrometeors indicated by asterisks and dots, respectively) lies the idealized 85-GHz PCT trace associated with each feature type. The schematic location of the 20-dBZ contour is labeled.

alent features excludes any link to rainfall occurring at PCTs ≥ 250 K.

d. Precipitation feature characteristic definitions

Once these precipitation features have been selected, quantifying their properties has been accomplished several ways, which will appear in the following sections. Six parameters have been used to quantify the structural differences between them: area, minimum PCT, maximum height of the 30-dBZ echo, maximum 6-km reflectivity, lightning frequency, and volumetric rainfall. Area is simply the number of data bins in a particular feature multiplied by the nominal area of a PR data bin. Minimum PCT is the minimum 85-GHz brightness temperature assigned to a feature after the nearest neighbor technique has matched TMI brightness temperatures to

the location of the PR data bins. Maximum height of the 30-dBZ echo is the greatest height the 30-dBZ echo extends above MSL in a system. This statistic has been linked to several convective intensity criteria, including updraft strength, rainfall intensity, and cloud-to-ground lightning frequency (Zipser 1994; Petersen et al. 1996). Also, DeMott and Rutledge (1998) reason that storms containing higher 30-dBZ heights likely contain more intense electric fields (and therefore more lightning), larger supercooled water and ice water contents; the second condition leading to lower 85-GHz PCTs.

Maximum 6-km reflectivity is defined as the highest reflectivity value in a feature in the radar bin 6 km above MSL. This statistic has been most notably correlated to a threshold for storm electrification by Dye et al. (1989). They reported that storms became electrically active when 6-km reflectivities (about $-10°$C) reached 40 dBZ.

TABLE 1a. Criteria used to classify the three TMI–PR-identified precipitation features from Mohr and Zipser (1996).

Category name	Data	Criteria
PF without ice scattering (≤250 K)	PR near-surface reflectivity and nearest neighbor TMI 85-GHz PCT (within the PR swath)	• 4 or more contiguous data bins (area ≥75 km²) with a PR near-surface reflectivity ≥20 dBZ • No data bins contain PCTs ≤250 K
PF with ice scattering and without an MCS	PR near-surface reflectivity and nearest neighbor TMI 85-GHz PCT (within the PR swath)	• 4 or more contiguous data bins (area ≥75 km²) with a PR near-surface reflectivity ≥20 dBZ or a PCT ≤250 K • At least one data bin with PCT ≤250 K • Does not meet the PF with an MCS criteria below
PF with an MCS	PR near-surface reflectivity and nearest neighbor TMI 85-GHz PCT (within the PR swath)	• 108 or more contiguous data bins (area ≥2000 km²) with PCT ≤250 K *with associated PR rain area* • 10 or more data bins (area ≥185 km²) with PCT ≤225 K

In addition, Zipser and Lutz (1994) showed that the distribution of derived 6-km reflectivities varied significantly among the tropical oceanic, midlatitude, and tropical continental storms observed. This provides additional justification of using 6-km reflectivities as a proxy indicator for lightning probability and convective intensity.

Lightning data from LIS is reported as point data, that is, the position of the flash is reported along with other retrieved parameters. The LIS instrument has the advantage that it views most locations within its swath for very nearly 90 s, so flash counts are linearly related to flash densities across the swath. All flashes within 8 km of a precipitation feature have been assigned to the closest feature data bin to give the number of flashes within 8 km of each precipitation feature. Volumetric rainfall is determined from the near-surface rainfall output from the 2A-25 algorithm (units of mm h⁻¹ km²). It uses a variational *Z–R* relationship that depends on the stratiform or convective classification of the PR data bin (among other parameters). This study only considers the relative rainfall contribution of each precipitation feature as a whole; there is no attempt to partition rainfall among convective and stratiform portions of the features.

3. Precipitation feature example

This section will present an example of several precipitation features and the interrelation of the datasets. Figure 2a presents a 0.67-μm visible image from the visible infrared scanner (VIRS) aboard TRMM, overlaid with PR near-surface reflectivity and collocated TMI 85-GHz PCT over Africa. The image is from 1455 UTC [~1500 local time (LT)] on 18 September 1998. There is a large contiguous area of deep convection apparent in the figure, as well as some isolated cells to the west of this line (near 10°N). The large feature extends well beyond the extent of the PR swath. However, this study acknowledges biases in the sampling of the areas of these features. The PR does, however, sample the vertical reflectivity and rainfall profiles within the swath. The large feature at the center happens to meet the MZ equivalent intense MCS criteria, with more than 108 contiguous data bins less than 225 K and more than 10 data bins less than 175 K. In this study, this system is classified as a precipitation feature with an MCS. This system appears to be a classic squall line system, with a leading convective line to the west and a large stratiform region extending eastward. An along-satellite track cross section of this feature, indicated by the "Ray 29 cross section" indication on Fig. 2a, appears in Fig.

TABLE 1b. Criteria used to classify the ice-scattering-only criteria from Mohr and Zipser (1996).

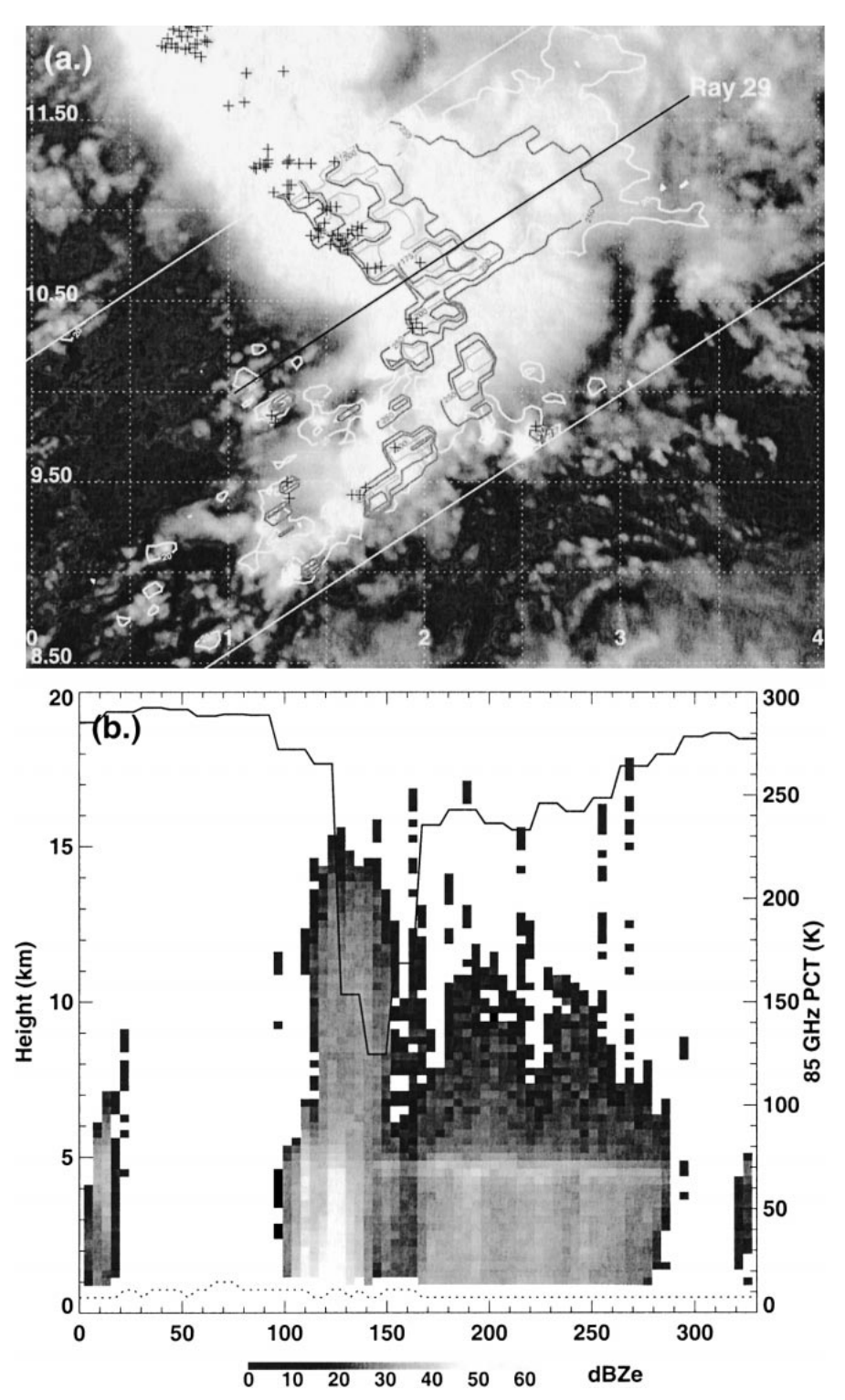| Category name	Data	Criteria
MZ equivalent MCS	TMI 85-GHz PCT only, within the PR swath	• 108 or more contiguous data bins (area ≥200 km²) with PCT ≤250 K *without associated PR rain area* • 10 or more data bins (area ≥185 km²) with PCT ≤225 K
MZ equivalent intense MCS	TMI 85-GHz PCT only, within the PR swath	• 108 or more contiguous data bins (area ≥200 km²) with PCT ≤225 K *without associated PR rain area* • 10 or more data bins (area ≥185 km²) with PCT ≤175 K

FIG. 2. (a) 1455 UTC 18 Sep 1998 VIRS visible image, overlaid with PR near-surface reflectivity (white, contoured at 20 and 40 dBZ), TMI collocated 85-GHz PCT (gray, contoured at intervals of 25 K beginning at 250 K), and LIS flash locations (+ symbols). The cross section in (b) is indicated by Ray 29 label. (b) Shaded PR reflectivity cross section through the precipitation feature with an ice scattering MCS pictured in (a).

TABLE 2. Number and percentage of total precipitation features classified by the criteria in Table 1.

Region	No. PFs No.	No. PFs without ice scattering No.	%	No. PFs with ice scattering No.	%	No. PFs with an MCS No.	%
Africa	12 838	9596	74.7	2904	22.6	338	2.6
South America	12 604	9775	77.6	2632	20.9	197	1.6
East Pacific	17 401	15 993	91.9	1233	7.1	175	1.0
West Pacific	29 668	25 909	87.3	3568	12.0	191	0.6
Total	72 511	61 273	84.5	10 337	14.3	901	1.2

2b. The left y axis gives the height of the shaded reflectivity features, while the right y axis indicates the 85-GHz brightness temperature at the position indicated by the reflectivity profile. This cross section gives a good example of a squall line's vertical structure. The deep leading convective line, transition zone, and stratiform region are all apparent as defined by Biggerstaff and Houze (1991). The brightness temperature trace is well correlated with reflectivity structures above the melting level (keeping in mind the parallax problem associated with the TMI's 52.1° incident angle), except in the transition zone where reflectivity weakens aloft while strong to moderate ice scattering remains in this zone. Features like the ones presented in this example will be quantified by their intensity, rainfall, and lightning distributions in the following sections.

4. Precipitation feature characteristics

a. Population, geographic distribution, and diurnal cycle

This study found 72 511 precipitation features within the TRMM August, September, and October 1998 dataset. Table 2 details the breakdown of the features into the subcategories given above. A large fraction (84.5%) of the features found do not contain ice scattering, with a higher portion of features over the ocean not containing a data bin with PCT ≤250 K. There is almost double the fraction of features with ice scattering over land, both features with ice scattering and MCSs. This indicates a higher likelihood of finding convective processes sufficiently vigorous to loft large ice particles into the mid- to upper troposphere over continental areas. Table 3 identifies the MZ equivalent MCSs and MZ equivalent intense MCSs to select precipitation features using only ice scattering criteria. Here we find more MZ equivalent MCSs than precipitation features with MCSs because it

TABLE 3. MZ equivalent MCSs and intense MCSs found in the TRMM precipitation feature population.

Region	MZ equivalent MCSs	MZ equivalent intense MCSs	% intense
Africa	373	36	9.7
South America	221	8	3.6
East Pacific	236	2	0.8
West Pacific	235	4	1.7
Total	1065	50	4.7

is possible to have multiple MZ equivalent MCSs (closed 250-K isotherms following the ice scattering definition) contained in one contiguous rain area. It was also found that 4.7% of the features were MZ equivalent intense MCSs, which is consistent with the 4% found by MZ (1996) that used an instrument with different spatial resolution (SSM/I).

Figure 3 indicates the geographic distribution of precipitation features that were identified in this study. The three figures from top to bottom indicate the location of features without ice scattering, features with ice scattering, and features with MCSs, respectively. It is apparent that these precipitation features occur in preferred locations in each geographic region. Over the ocean, the ITCZ is a favorable environment for deep convection, while there seems to be less focusing over the land regions. Over Africa, regions from 10°S northward to the north boundary of the box contain the lion's share of the MCS activity in that region. In South America, features with ice scattering seem to favor the western side of the continent during this season, away from the Atlantic coast. The foothills of the Andes Mountains seem to be a focusing mechanism for MCSs. Central Africa contains the greatest concentration of intense convection found in the dataset. The bulk of the east Pacific's MCSs are near 10°N, near where the Northern Hemisphere warm season ITCZ is found. This is true to a lesser degree over the west Pacific, where MCSs cover a much broader area.

The diurnal cycle of precipitation features by type was investigated for the four regions sampled. The local time of observation of each feature was placed in 2-h bins centered on the odd hours of the day. The relative frequency of all precipitation features and relative frequency partitioned by each precipitation feature type within each 2-h bin is plotted in Fig. 4. The continental regions' features show a strong afternoon response to daytime solar forcing and associated low-level destabilization. Examination by feature type indicates that the features without ice scattering rise in frequency first during the daytime (1000–1200 LT), followed by features with ice scattering rising 2–4 h later. Both these features peak in frequency near 1400–1600 LT, and diminish slowly throughout the local evening. For precipitation features with an MCS, frequencies rise later in the afternoon than for smaller features, beginning between 1400 and 1600 LT over both regions, remaining
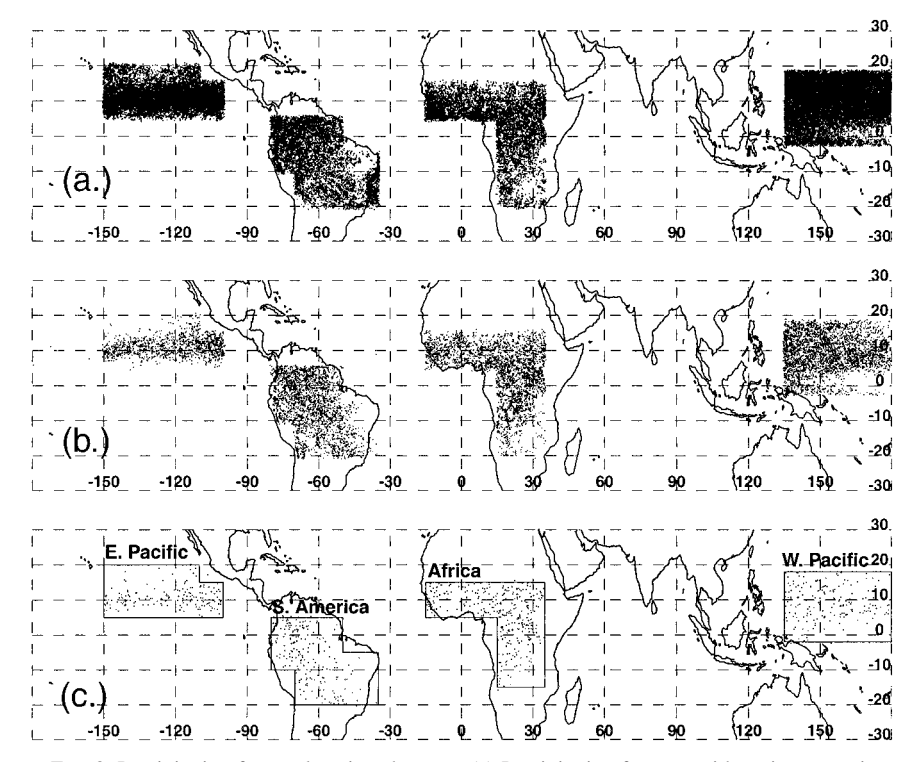
FIG. 3. Precipitation feature locations by type. (a) Precipitation features without ice scattering, (b) precipitation features with ice scattering, and (c) precipitation features with an MCS are indicated by a small dot. The boundaries of the four analysis regions used in this study are shown in (c).
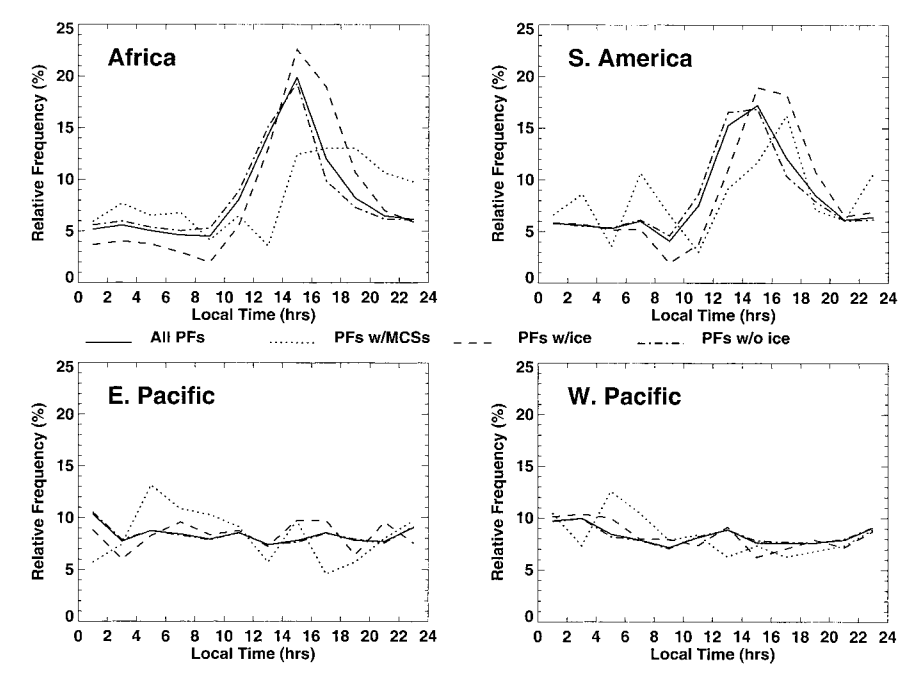
FIG. 4. Diurnal cycle (in 2-h local time bins) of TRMM precipitation features over the four analysis regions. Solid line indicates the relative frequency of all precipitation features, while dotted, dashed, and dash–dotted lines indicate the relative frequency of precipitation features with MCSs, with ice scattering, and without ice scattering, respectively.

TABLE 4. Selected physical characteristics of the precipitation features.

Region/type	No. of TPFs	Median area (km^2)	Median min PCT (K)	Median max height of 30-dBZ echo (km)	Median max 6-km reflectivity (dBZ)
Africa (all PFs)	12 838	166	268	4.75	22.9
Without ice scattering	9596	130	272	4.5	19.1
With ice scattering	2904	684	220	7.75	37.9
With an MCS	338	10 946	138	12.5	45.5
South America (all PFs)	12 604	148	271	4.75	19.9
Without ice scattering	9775	130	274	4.25	16.7
With ice scattering	2632	647	225	7.25	36.2
With an MCS	197	10 539	150	11.25	44.4
East Pacific (all PFs)	17 401	148	281	1.75	0.0*
Without ice scattering	15 993	130	281	1.5	0.0*
With ice scattering	1233	1553	231	5.5	28.4
With an MCS	175	19 914	176	7.0	34.4
West Pacific (all PFs)	29 668	129	279	3.25	15.3
Without ice scattering	25 909	111	281	3.0	13.8
With ice scattering	3568	684	228	6.25	31.4
With an MCS	191	15 846	163	8.5	39.2

* Median reflectivity value of 0.0 indicates the value is lower than the minimum detectable signal of the PR (~15 dBZ).

steady throughout the evening over Africa until midnight, but diminishing quickly by 2200–2400 LT over South America. During nocturnal hours, there is a hint of an overnight second maxima of MCSs over both regions (0200–0800 LT); however, the reader should be strongly cautioned of the small number of MCSs observed in this study (especially when divided among 12 diurnal bins).

Over the ocean, there is a weak diurnal signal among precipitation features. Excluding MCSs, there is never more than a 2%–3% deviation in the relative frequency of feature-type observations, with a slight rise in activity among the non-MCS systems in local nighttime between 2000 and 0200 LT. MCSs show a relative peak in activity in the 0400–0600 LT bin, with a relative minima in the local afternoon. Again, caution must be used when interpreting the MCS diurnal cycle, as there are less than 200 precipitation features with an MCS divided among 12 time bins in each oceanic region. These findings agree qualititively with the findings of Chen and Houze (1997) and Hall and Vonder Haar (1999), who used IR satellite brightness temperatures to identify an overnight maximum in the spatially large, long-lived precipitation features in the west Pacific warm pool.

The previous works using the SSM/I to classify precipitation features (MZ 1996; Mohr et al. 1999; and

others) relied on the sunrise/sunset orbital pattern of the Defense Meteorological Satellite Program (DMSP) satellite. Not only does this orbital pattern not enable sampling of the complete diurnal cycle, but it also integrates bias into the estimation of the frequency and rainfall from different classes of systems. By sampling at 0600 and 1800 LT only, it is evident from Fig. 4 that a significant portion of the precipitation features not meeting MCS criteria are missed over land due to the SSM/I's observation times. This may have important implications on the SSM/I's ability to obtain a representative sample of precipitation features and to estimate their rainfall and intensity free of diurnal cycle bias effects.

b. Structure statistics

Table 4 gives median values of the four statistics used to compare storm characteristics among the regions and four types of systems. Table 5 summarizes the statistics for the MZ equivalent MCSs. Given are the median values of feature area, minimum PCT, maximum height of the 30-dBZ contour above mean sea level, and maximum reflectivity at 6 km above mean sea level.

1) AREA

Median precipitation feature area statistics (Table 4) show that these systems are comparable in size when all features are taken into account (within three PR data bins in size for all features), but when the more intense systems are compared, these features are significantly larger over the ocean. For precipitation features containing MCSs, for example, features size is about 1.5–2 times larger comparing the west Pacific (15 846 km^2) and the east Pacific (19 914 km^2) to the continental regions (10 946 and 10 539 km^2 for Africa and South America, respectively).

TABLE 5. Selected characteristics of the MZ equivalent MCSs and intense MCSs.

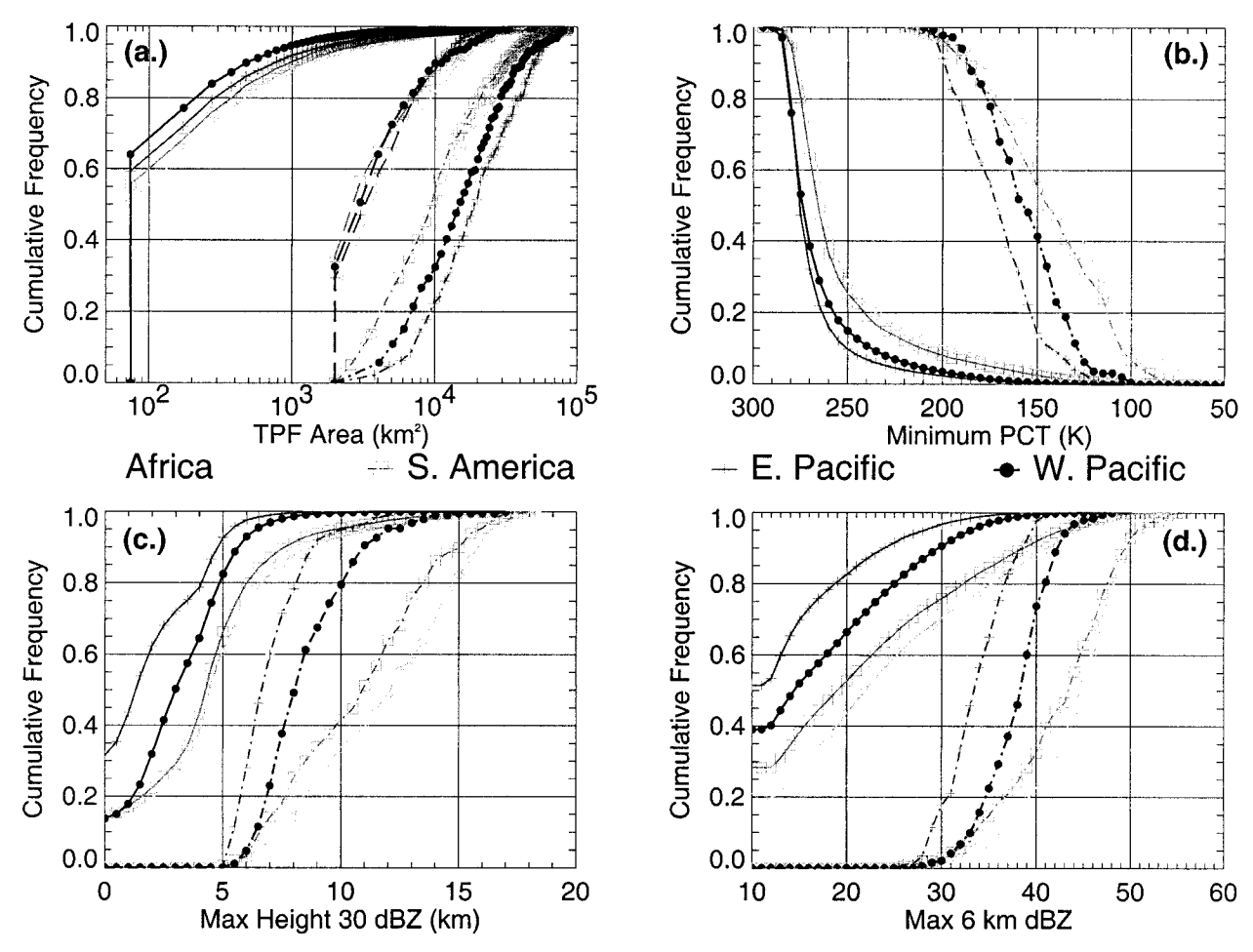| Region	Median area (km^2)	Median min PCT (K)	Median max height of the 30-dBZ echo (km)	Median max 6-km reflectivity (dBZ)
Africa	4530	140	11.75	43.7
South America	3716	154	10.25	41.5
East Pacific	4234	183	6.5	33.1
West Pacific	3975	169	7.75	37.1

FIG. 5. (a) CDFs of precipitation feature area (solid), MZ equivalent MCS area (long dash), and precipitation feature with MCS area (dash–dot). Also, CDFs of (b) minimum PCT, (c) maximum height of the 30-dBZ echo, and (d) maximum 6-km dBZ for all features (solid) and features with MCSs (dash–dot).

The area statistics in Table 5 considers only the MZ equivalent MCSs. The area enclosed by the 250-K PCT isotherm leads to similar area values between regions. This suggests that over the ocean the most intense systems contain a larger area of rainfall outside the 250-K isotherm, but do not contain a larger area of the more intense ice scattering and rainfall occurring ≤250 K. This, along with higher ratios of features without ice scattering to features with ice scattering over the ocean suggest that there is more rainfall occurring at higher PCTs over ocean than over land.

For all precipitation features (Fig. 5a), area distributions among all feature types are similar in shape, with a large number of small systems dominating the dataset. Continental regions have slightly larger systems at a given percentile than oceanic systems. The area distributions for features with MCSs include the area of ice scattering (≤250 K) and the associated rainfall outside the scattering area. It is apparent that the ocean systems are larger at a given percentile, consistent with the median statistics that were discussed above.

Areas of the systems as defined by MZ equivalent criteria (PCT ≤ 250 K) do not reflect this size difference. *Rain areas of the systems as defined by ice scattering signatures alone are not similar in size.* This contradiction between the areas contained in MZ equivalent MCSs and the total area of rain surrounding them supports the hypothesis that a higher fraction of rain is falling at higher PCTs over oceanic regions. This will be examined further when rainfall distributions are discussed below.

Area distributions of precipitation features are limited by the 215-km swath width of the PR. Tables 6 and 7 give the number and percentage of precipitation features and MZ equivalent MCSs and intense MCSs, respectively, that are truncated by the edge of the swath. In all, about 17% of all precipitation features were artificially cut by the swath, with the more intense (and larger) systems truncated more often (82% for features with MCSs). Many times, only the rain area outside the MZ equivalent MCS area was cut; only 54% of the actual MZ equivalent MCS areas ≤250 K were sliced. This

TABLE 6. Narrow swath effects on precipitation features.

Region	PF total		PF without ice scattering		PF with ice scattering		PF with an MCS	
	Edge of swath	%	Edge of swath	%	Edge of swath	%	Edge of swath	%
Africa	2731	21.3	1445	15.1	1013	34.9	273	81.0
South America	2465	19.6	1399	14.3	905	34.5	161	82.1
East Pacific	2723	15.6	1928	12.1	628	50.9	167	95.4
West Pacific	4314	14.7	2888	11.3	1252	35.1	174	91.1
All regions	12 233	17.0	7660	12.6	3798	36.8	775	86.2

limitation causes some truncation of the area distribution of precipitation features, but this distribution is accurate and unbiased in its portrayal of 1) a greater number of small systems compared to the number of large systems and 2) broader systems over the oceanic regions when comparing the larger, more intense systems. This edge of swath effect does not cause a systematic bias in the comparisons of storm structure that appear in the following sections. However, since the rain areas associated with precipitation features with MCSs are more likely to be truncated than the MZ equivalent MCSs themselves, this likely causes an *underestimate* in the land/ocean difference in rain areas outside features with MCSs.

2) MINIMUM PCT

The following three parameters use TMI and PR observations to compare intensities among the precipitation features. MZ (1996) analyzed minimum PCTs of ice scattering MCSs. It was found for the sunset passes of the SSM/I that at the 10th percentile of storms by intensity (as measured by their low 85-GHz temperatures), continental MCSs had minimum PCTs about 25 K lower than their oceanic counterparts. TRMM presents many advantages over the SSM/I in this comparison. Ability to sample throughout the diurnal cycle, the PR's sampling beyond the microwave signature, and increased passive microwave resolution enables TRMM to better differentiate among storms by intensity.

Table 4 reveals that continental regions produce significantly lower median values of precipitation feature minimum PCT than oceanic storms for all categories. This varies by type from 11 to 13 K for all precipitation features to near 30 K for features with MCSs. The MZ

TABLE 7. Narrow swath effects on the MZ equivalent MCS and intense MCSs.

Region	MZ equivalent MCS		MZ equivalent intense MCS	
	Edge of swath	%	Edge of swath	%
Africa	217	58.2	11	30.6
South America	114	51.6	6	75.0
East Pacific	129	54.4	2	100.0
West Pacific	118	50.0	0	0.0
All regions	578	54.3	19	38.0

equivalent MCSs alone (Table 5) also demonstrate this distinct difference in median intensity between land and ocean storms (~40 K between Africa and the eastern Pacific). Differences (~12 K among MCSs) also exist when examining Africa versus South America and east versus west Pacific. Figure 5b contains a cumulative distribution function (CDF) of precipitation feature minimum PCT (solid line). While there is a "modest" PCT difference at the 50th percentile of storms (~12 K), the 90th percentile reveals a 40–45-K difference between land and ocean storms. Removing the weak systems over all regions can be accomplished by looking at features with MCSs distributions. These features are shown by the dash–dot line in Fig. 5b. Here there is a 40–45-K difference between the land and ocean storms consistently below the 60th percentile. This suggests that, in their most intense ice scattering cores, these continental precipitation features and MCSs contain a significant additional optical depth (by size or concentration) of ice. This is particularly apparent in the stronger systems in the precipitation feature distribution and the MCSs. Mohr et al. (1999) shows a 30–40-K difference at the intense percentiles among the ice scattering MCSs sampled with the SSM/I, which shows consistency with this study.

3) MAXIMUM HEIGHT OF THE 30-DBZ ECHO

Median values of the maximum height of the 30-dBZ echo appear in Tables 4 and 5. For continental regions' precipitation features, this parameter takes the value of 4.75 km above MSL for both Africa and South America, while over the oceanic regions the height is much lower (1.75 and 3.25 km for the east and west Pacific, respectively). This is accentuated in data for the features with MCSs, where the median values are 2.5–5.5 km higher for continental regions than over the oceans. Figure 5c shows the feature distribution of the maximum height of the 30-dBZ echo. Again, continental regions show higher 30-dBZ echo heights for the most intense convective data bins, extending about 3 km higher, on average, at the 90th percentile (see Fig. 5c, solid line). The east Pacific region's distribution has a different shape than the other three; this is likely due to the large number of features without ice scattering found in the northern part of the analysis region (Fig. 3). The larger number of precipitation features without ice scattering

over the ocean (which must have weaker reflectivity profiles above the melting level) likely diminishes the range of the distribution of the 30-dBZ heights over the ocean.

Again to remove the weaker systems from the comparison, the dash–dot portion of Fig. 5c shows the maximum 30-dBZ echo heights for precipitation features with MCSs over the study regions. The oceanic distributions become more similar in shape in this plot, with the east Pacific still containing the lowest echo heights. Here there is a distinct difference in the shapes between land and ocean regions. Ocean regions' MCSs 30-dBZ echo heights remain below 10 km for most of the spectrum, but land convection rises to near 15 km by the 90th percentile.

Despite similarities between the land regions and between the ocean regions themselves, there are notable differences between them. African precipitation features with MCSs consistently contain 1–2 km higher maximum heights of the 30-dBZ echo than South American ones at a given percentile. Also, the distribution of east Pacific region maximum heights of the 30-dBZ echo show many differences compared to the west Pacific. For example, 70% of east Pacific systems have max 30-dBZ echo heights less than 3 km. Compare this to only 40% of the systems over the west Pacific being weak enough to contain the maximum 30-dBZ echo heights less than 3 km. This highlights a few of the significant differences between the individual regions that need further investigation.

4) MAXIMUM 6-KM REFLECTIVITY

Tables 4 and 5 again reveal consequential differences in 6-km reflectivity structure among the land and ocean systems. For all precipitation features, continental systems exhibit more than 4 dBZ higher median reflectivities at 6 km than ocean systems. Note that over the east Pacific, precipitation features without ice scattering contained such weak reflectivities at 6 km as to be below the minimum detectable signal of the PR at the median level. Because these systems were so numerous, they pushed the median reflectivity for all features in that region below the minimum signal. For the MCSs, continental median maximum 6-km reflectivities exceeded oceanic ones by 5–10 dBZ. Figure 5d's solid portion shows a CDF of maximum 6-km reflectivities for all precipitation features. Between 20%–52% of the features, depending on the region, do not have reflectivities above the PR minimum detectable reflectivity. This is especially apparent over the east Pacific box. However, once systems extend above this intensity level, the continental systems are again stronger by several dBZ. For the MCSs, Fig. 5d (dash–dot) shows maximum 6-km reflectivity differences at or exceeding 10 dBZ throughout the distribution above about the 30th percentile. This clearly shows that the continental updrafts are lofting much larger concentrations of hydrometeors to higher

TABLE 8. Number of lightning flashes within 8 km of each precipitation feature category.

Region	PF without ice scattering	PF with ice scattering	PF with an MCS	Total
Africa	388	11 819	12 796	25 003
South America	251	8815	5260	14 326
East Pacific	0	40	45	85
West Pacific	7	138	127	272
Total	646	20 812	18 228	39 686

altitudes in these intense systems. Again, differences among the land and ocean regions themselves are apparent. Here there is nearly as much difference between the east and west Pacific as there is between the west Pacific and the continental regions.

These land–ocean differences indicate that despite oceanic precipitation features with MCSs containing significantly more rainfall *outside* the 250-K contour, they are much weaker and likely contribute differently to the heating and moisture budgets than those systems over land. The larger number of features without ice scattering over the ocean (which are likely be shallow in order to avoid scattering radiation at 85 GHz) will be shown to contribute much more to the total rainfall over these regions.

c. Lightning statistics

With LIS aboard TRMM, it is possible to calculate the contribution of each precipitation feature type to the total lightning observed from the sample of features. Knowing the intensity distributions of the precipitation features from the preceeding analysis can help to explain the observed lightning patterns. LIS recorded 39 686 flashes within 8 km of precipitation features during the 3-month period. The contribution to the total lightning observed by region and by feature type is presented in Table 8. There is nearly two orders of magnitude difference betwen lightning in land and ocean regions in the statistics. This lightning ratio of approximately 100:1 holds for all types of features analyzed in the dataset. There is about one-third more lightning contained within precipitation features with ice scattering than with an MCS.[3] Even when considering the largest of features by median area, the oceanic features with an MCS, only 136 flashes occurred from 366 features, compared with 13 519 flashes for 535 features with MCSs over land. Clearly, the intensity differences quantified above have crucial implications on the lightning probability for a given oceanic or continental MCS.

---

[3] Also note that 61 273 precipitation features without ice scattering produce a total of 646 flashes, with all but 7 of those occurring over land. (We interpret this result to mean that the features that do produce lightning in this category possibly contain an ice scattering signature but that it is too spatially small to be quantified at TMI resolution.)
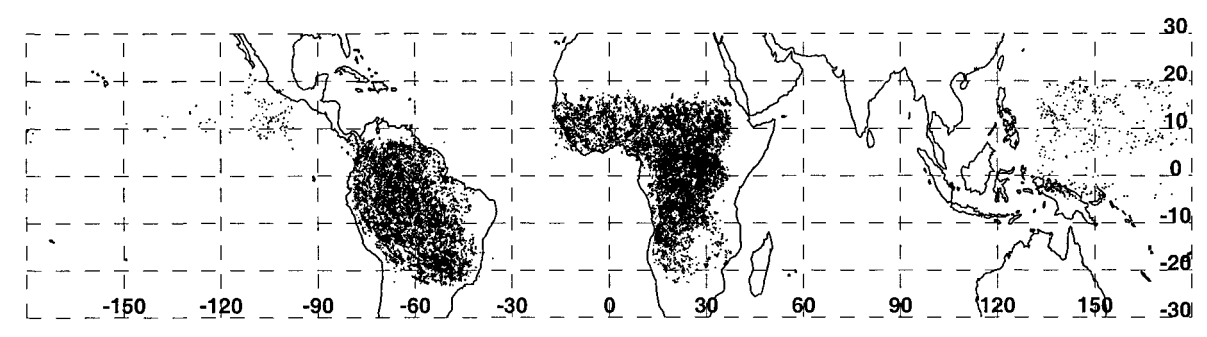
FIG. 6. Locations of lightning associated within 8 km of precipitation features for the four analysis regions.

Figure 6 plots the geographic distribution of the flashes in each region. It is apparent that over the ocean there is a clustering of lightning north of the equator in agreement with the climatological position of the ITCZ (as shown by the presence of precipitation features in Fig. 3). The evident high concentrations of lightning over land dominates the total amount of lightning observed.

To further quantify the distribution of flashes per system, Table 9 quantifies the regional number of precipitation features in each category containing no flashes, between 1–9 flashes, 10–99 flashes, and more than 100 flashes. Between 9% and 12% of precipitation features with ice scattering over land contain 10 or more flashes, while only 83 out of 4801 features (1.7%) with ice scattering contain even one flash (with 3 containing 10 or more). Thirty-nine of Africa's 338 precipitation features with MCSs contain more than 100 flashes, while South America only has 7 out of 197 meeting such criteria. Only 4 oceanic MCSs contain 10 or more flashes, with none containing more than 100.

The last column in Table 9 shows the number of feature data bins (as a proxy for area, each data bin is 18.5 km^2) per lightning flash in each region by feature type. Precipitation features without ice scattering show the same trend as before, containing a large area of rainfall per flash. Except over the west Pacific, precipitation features with ice scattering contain less rain area per flash than features with MCSs. This is likely due to the larger fraction of stratiform rain contained in MCSs
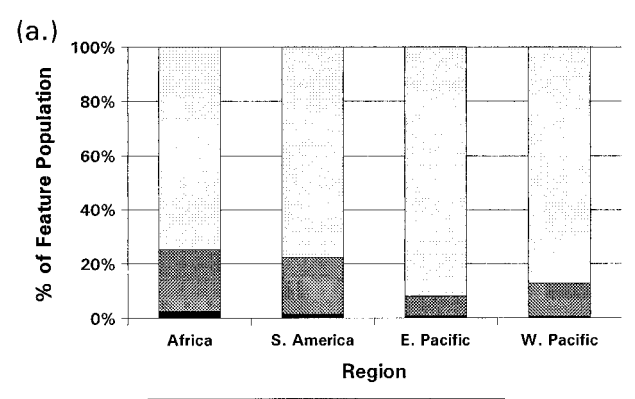
compared with smaller multicell storms (Houze 1993), thus containing lower flash rates. Oceanic systems with ice scattering and MCSs contain about 150 times more rain area per flash than features over land. This again highlights the differences in intensity as observed by the other TRMM instruments. It is also interesting to note that over the ocean, only about 0.3% of the precipitation features contain lightning, while over land 14.1% contain lightning.

d. Rainfall statistics

As mentioned above, the TRMM PR 2A-25 algorithm rainfall estimate was used to quantify the rainfall contribution of each feature. This section presents the contribution of each classification of feature to the total rainfall measured during this analysis period. Again, note that there is no attempt to separate rainfall among stratiform or convective areas within precipitation features. Figure 7a shows the relative abundance of precipitation features by type as classified in Table 1. Note that precipitation features without ice scattering are more abundant over the ocean, accounting for 92% of features over the east Pacific, for example. Features with ice scattering are more profuse over the continental regions, accounting for 20%–25% of the features. MCSs are quite rare, accounting for less than 3% of the total features by number over all regions. As one would expect, the smaller systems must contribute less to total

TABLE 9. Lightning frequency observations from the precipitation feature types.

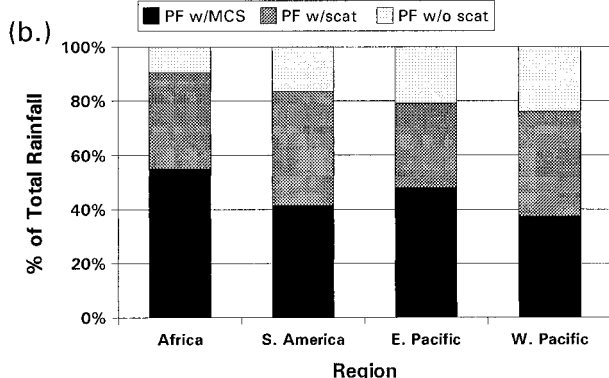| Region	Feature type	Without any flashes	With 1–9 flashes	With 10–99 flashes	With ≥100 flashes	Number of data bins per flash
Africa	Without ice scattering	9377	219	0	0	291
	With ice scattering	1369	1182	351	1	20
	With an MCS	44	22	194	39	22
South America	Without ice scattering	9624	150	1	0	445
	With ice scattering	1388	984	258	1	22
	With an MCS	29	41	113	7	29
East Pacific	Without ice scattering	15 993	0	0	0	∞
	With ice scattering	1217	15	1	0	5255
	With an MCS	160	14	1	0	5337
West Pacific	Without ice scattering	25 902	7	0	0	35 836
	With ice scattering	3501	65	2	0	2051
	With an MCS	166	22	3	0	1683

(a.)

(b.)

FIG. 7. Contribution by each feature category to (a) total feature
population and (b) total regional rainfall.

rainfall than they do by number, and that is shown in
Fig. 7b. This figure shows the percentage of the total
volumetric rainfall for each type of system in each re-
gion. The features without ice scattering contribute only
9% of the rainfall in Africa, with a maximum of 23%
over the west Pacific. It appears that these weak systems
are a more important contributor to the rainfall over the
ocean, with their contribution related to their relative
population. Despite features with some ice scattering
accounting for about twice the percentage over the land
areas than over the ocean, their contribution to rainfall
is roughly the same over both land and ocean. Features
with MCSs contribute 38%–55% of the total rainfall in
the various regions. It is especially noteworthy that just
1.5% of the systems are contributing about *half* the
rainfall in a given region. Likewise, precipitation fea-
tures meeting MZ intense MCSs criteria (but containing
the associated ''warm'' rainfall) contribute much more
in precipitation than they do in number. The 35 precip-
itation features with MZ intense MCSs (0.3% by num-
ber) contribute 12% of the total African box rainfall
(not shown).

In order to further quantify the distribution of rainfall
from the precipitation features found in this study, an
examination of the rainfall from features according to
their estimated intensity follows. Features will be par-
titioned by their minimum PCTs and maximum heights

of the 30-dBZ echo to compare differences among the
regions' precipitation features.

1) RAINFALL BY MINIMUM PCT

Figure 8 is a CDF of precipitation feature rainfall
according to their minimum PCT for each region. For
the PCT CDFs, the scale has been reversed to indicate
increased ice scattering intensities to the right (decreas-
ing brightness temperatures). The curves have been con-
structed using 10-K PCT intervals plotted at the mini-
mum PCT contained in that interval. For each of the
following categories, precipitation features without ice
scattering (diamonds), precipitation features with ice
scattering (plus symbols), and precipitation features
with MCSs (filled circles), the CDF of features by their
minimum PCT (dashed line) and the relative rainfall
contribution by those features is plotted (solid line).
Subtracting the dashed from the solid curve for a given
system type yields the difference in the contribution to
the population and the total rainfall distributions at a
given PCT range. For example over the east Pacific,
there is about a 25% difference between the number and
rainfall distributions at 260 K. Looking at the drop in
either distribution over a given range indicates the rel-
ative occurrence of features in that bin. Again over the
east Pacific, the almost 60% difference between the 280-
and 270-K minimum PCT bins in the feature without
ice scattering number distribution show the large num-
bers of features in this category. However, these features
only account for less than 25% of the rainfall in the
category.

For each region, there are shape similarities in the
minimum PCT number and rainfall distributions. There
are significant differences, especially when comparing
the intensities of the features. Over the ocean, features
without ice scattering occupy a sample space about 10–
20 K higher than over land. The 270–280-K range con-
tains more than half of these features over the ocean,
while these weak features are most likely located in the
260–270-K bin over land. For both land and ocean,
rainfall is more likely to originate from features with
more ice scattering, as evidenced by the rightward shift
in the rainfall distribution.

Precipitation features with ice scattering range to
much lower PCTs over land than ocean. By number,
both Africa and South America have about 20% of fea-
tures containing ice scattering signatures less than 175
K. Over the ocean, this part of the distribution is more
nearly 190 K. This has implications on the rainfall dis-
tribution. For all of the regions, there is a 15%–25%
difference in the number and rainfall distributions for
most minimum PCTs. However, the larger number of
intense features over land shifts the rainfall distribu-
tions. For example, between 20% and 25% of the con-
tinental rainfall comes from features with minimum
PCTs less than 150 K, compared with less than 10% of
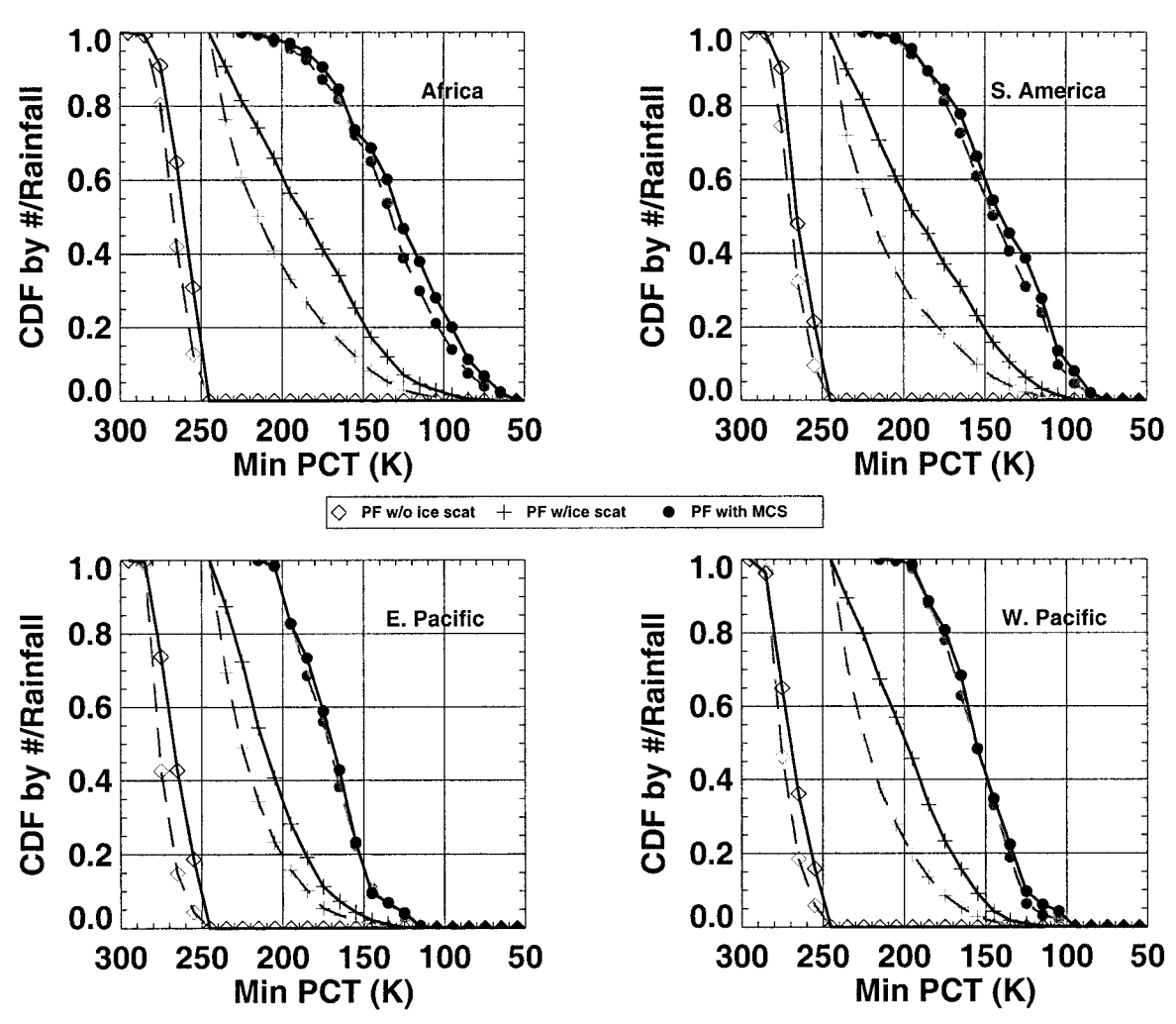oceanic rainfall. Note that these features do not meet

FIG. 8. CDF of number (dashed) and rainfall (solid) by minimum PCT for the four analysis regions by system type (see legend).

MCS criteria, so these small features are more intense over land, with more rainfall coming from these stronger features.

For MCSs, again there is a significant regional difference in the intensity distributions, with a significant portion of the features below 100 K over land. However, the rainfall distributions are very similar to the population distributions, indicating that minimum PCT is not a significant indicator of rainfall in these large systems where certain intensity criteria have been already satisfied. However, there seems more of a difference among the two distributions over land, indicating more of a peak intensity–rainfall relationship.

2) RAINFALL BY MAXIMUM HEIGHT OF THE 30-DBZ ECHO

As in the previous section, here (Fig. 9) number and rainfall distributions are analyzed for the precipitation feature types, but by the maximum height of the 30-dBZ echo. Like the maximum 6-km reflectivity, this

parameter presents a scale of feature intensity independent of the criteria used to define the features themselves. DeMott and Rutledge (1998) analyzed the maximum 30-dBZ echo heights and rainfall during TOGA-COARE in the west Pacific warm pool and found oceanic peaks in the number distribution of 30-dBZ heights at 4–5 km with peaks in the rainfall distribution according to 30-dBZ heights at 5–6 km (their Figs. 5 and 6). From TRMM, it is again apparent that there is large number of weak, shallow features that contribute little toward the total regional rainfall compared to the deeper systems (Fig. 9).

There is a large number (33%) of very shallow precipitation features without ice scattering over the east Pacific with a 30-dBZ echo height of 1 km or less that contribute 10% of the rainfall in that region. Over land, about 90% of the features without ice scattering have maximum 30-dBZ echo heights less than 7 km. The 90th percentile lowers to about 5 km over the west Pacific and 4 km over the east Pacific. This independently shows that these features without ice scattering ($\leq$250
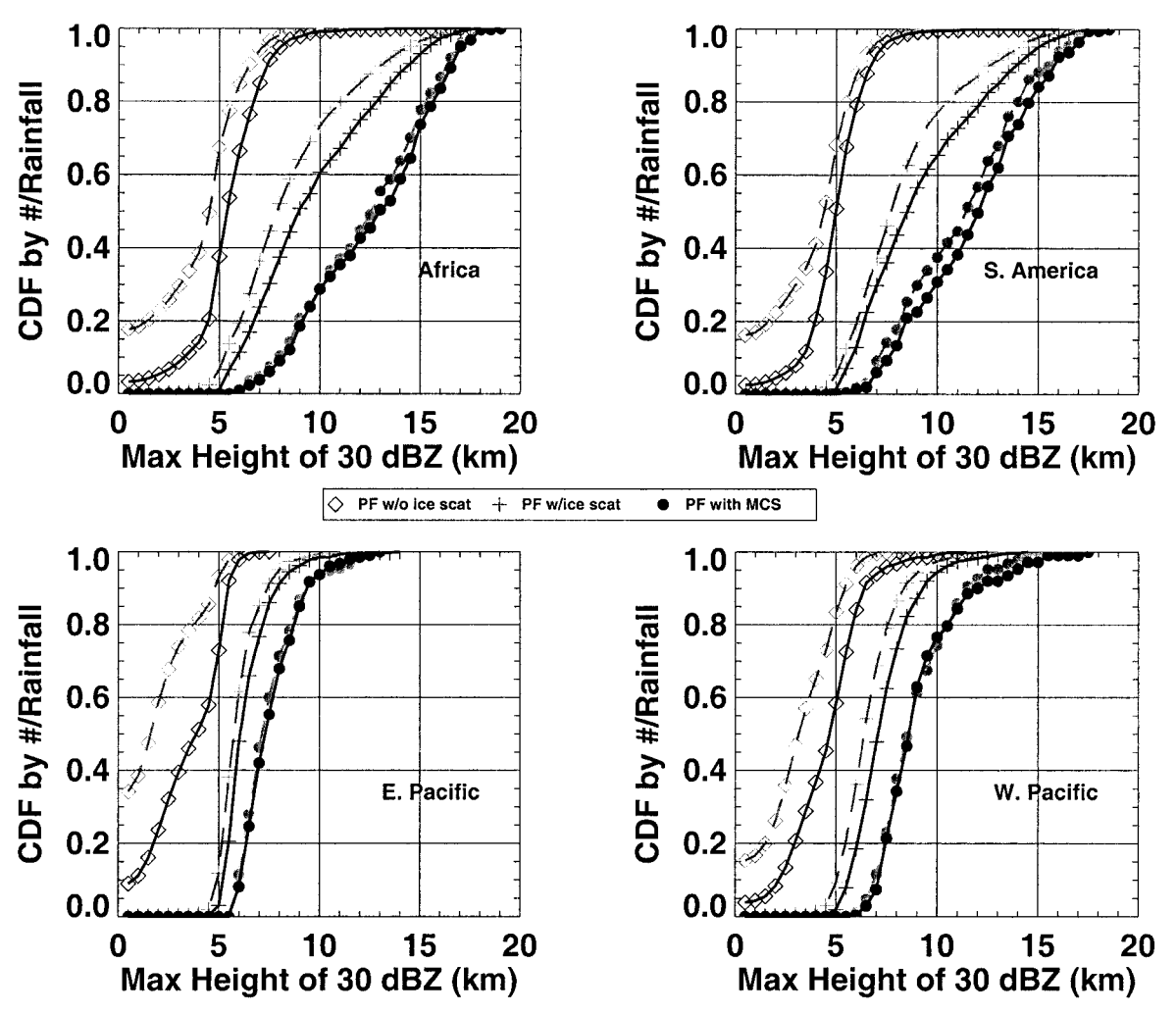
FIG. 9. CDF of number (dashed) and rainfall (solid) by the maximum height of the 30-dBZ echo for the four analysis regions by system type (see legend).

K) are indeed shallow reflectivity features with relatively little mass above the freezing level. Also note the differences in the shapes of the distributions among the regions, which is more significant than the PCT distribution differences. This difference is apparent in the other classifications and is likely due to the fact that echo height is not a criteria in precipitation feature selection and is not reflected in the sample selection in any way. For all distributions, it is clear that the very shallow features do not contribute to the rainfall significantly despite their abundance.

Precipitation features with ice scattering can range from somewhat shallow features (with maximum 30-dBZ echo heights around the freezing level) to very deep convective features that just did not meet MCS criteria. Number and rainfall distributions over the ocean are much steeper than over land, indicating the rarity of the deep features (with the maximum 30-dBZ height ≥ 10 km) over water. By percentile, rainfall is contributed more by deeper features over the land than over the

ocean (as portrayed by the wider gap between the number and rainfall curves). As with the PCT classification, MCSs seem to contribute to the rainfall proportionately by their abundance. Land and ocean differences in intensity are apparent, but South America is the only region that shows a significantly increased contribution to rainfall from deeper features. These results show that peak intensity (i.e., minimum or maximum) values may not be the best indicator of rainfall parameters (especially for MCSs).

These rainfall distributions elucidate several key points about differences in rainfall among the regions sampled in this study. Despite oceanic regions containing more systems, a large number of these produce little rainfall. The intense features over the ocean that produce the bulk of the rainfall tend to reach minimum PCTs between 175 and 225 K and have maximum 30-dBZ echo heights between 5 and 9 km. Land features producing most of the rainfall have more widely varying properties; contribution to rainfall is spread out over a

range of lower minimum PCTs and echo heights reaching greater heights than the oceanic systems.

5. Conclusions and future work

The precipitation features examined using TRMM over differing regions of the Tropics have several distinguishing features. This 3-month dataset contained over 70 000 precipitation features, with about 90% and 80% of those over ocean and land, respectively, contained no TMI 85-GHz PCTs less than 250 K. Features with and without ice scattering were numerous when compared to the number of precipitation features containing MCSs (around 1% of the total number over all regions except Africa, which contained 2.6%).

Important differences were found in the intensity and rainfall patterns of land versus ocean convection. Area distributions revealed that when all precipitation features were accounted for, similar area distributions were found for all regions, with continental regions having slightly larger areas. The MZ equivalent MCSs (when considered only for their area with PCT $\leq$250 K) exhibited a similar pattern with continental systems having larger areas. When the rain area associated with the MCSs were investigated, this pattern reversed with oceanic intense systems containing a larger area of rainfall than systems over land. With this rain occurring at high brightness temperatures at 85 GHz (i.e., little ice scattering), increased ambiguity is introduced in ice scattering-based precipitation retrieval. This highlights the inherent uncertainties in using ice scattering methods in estimating light precipitation, or heavy rainfall occurring at small spatial scales or without a significant ice scattering signature.

Using properties retrieved from the PR, differences in reflectivity structure among the regions could be quantified. With significantly higher values of maximum 6-km reflectivity and maximum height of the 30-dBZ echo, land convection was shown to be significantly stronger than convection over the ocean, with Africa having the strongest and the east Pacific containing the weakest. This was also reflected in the minimum PCT distributions that signaled much more ice mass aloft in continental features. This was shown to a higher degree when the larger (and likely more intense) storms (MCSs) were taken into consideration. All this information supports hypotheses about the lack of lightning over the ocean being linked to slower updraft speeds unable to create large optical depths of ice above the melting level.

Implications of the differing intensity parameters observed on the rainfall distribution were examined. Despite similar retrieved rainfall amounts over the four regions when normalized by area, the modes of rainfall were very different when comparing the regions. The oceanic regions had significant rainfall contribution from a large number of warm systems without significant ice scattering. Again, these features are either warm rain features in the classic definition, features with in-

sufficient ice processes to lower PCT below 250 K, or smeared systems too small to be resolved by TRMM resolution. The second mode of oceanic rainfall comes from large, moderately intense systems with ice scattering. These systems are almost never intense enough to produce lightning, but do produce heavy rainfall. Over continental areas, the bulk of the rainfall comes from a broad spectrum of moderately strong to very intense features, with more of the rainfall coming from areas with lower minimum PCTs and higher maximum heights of the 30-dBZ echoes than over the ocean. Rainfall from smaller systems was a more direct function of their intensity than for stronger systems, for which rainfall was a function of their abundance and size. In spite of differences in the rainfall distributions for the storms, lightning flash densities for storms with similar rainfall followed similar distributions over both regions. This related the crucial need for more detailed microphysical study and modeling in comparing land and ocean storms. This may be done with more detailed analysis of the TRMM satellite and ground validation dataset, which can aid in improving conceptual and numerical models.

Future work will include a more detailed examination of the reflectivity and passive microwave signatures of precipitation in the Tropics. Full datasets of radar reflectivity profiles as well as multiple TMI channels will be used to more closely investigate hypotheses about microphysical differences in convection throughout the Tropics. Also, high-resolution aircraft and ground-based reflectivity, cloud physics, and other environmental measurements obtained in recent TRMM field campaigns can be used to aid in answering questions about storm structure and microphysics.

Future work in progress includes expanding the temporal and spatial dimensions of the TRMM precipitation feature dataset throughout the Tropics to examine precipitation features measured during the first two years of the satellite's operation. A larger dataset will allow the investigation of diurnal cycle issues in depth, a larger regional comparison, and a more detailed comparison of the structure of precipitation features (i.e., convective versus stratiform properties). Also, incorporating the LIS data in a more quantative manner will allow the testing of lightning–ice scattering–radar reflectivity relationships throughout the Tropics. In addition, the generation of detailed, high-resolution case studies from the TRMM field programs of 1998–99 will allow those observed precipitation features to be placed in the context of the Tropicswide TRMM precipitation feature dataset.

REFERENCES

Biggerstaff, M. I., and R. A. Houze Jr., 1991: Kinematic and precipitation structure of the 10–11 June 1985 squall line. *Mon. Wea. Rev.,* **119,** 3034–3065.

Chen, S. S., and R. A. Houze Jr., 1997: Diurnal variation and life-cycle of deep convective systems over the tropical Pacific warm pool. *Quart. J. Roy. Meteor. Soc.,* **123,** 357–388.

Christian, H. J., 1999: Optical detection of lightning from space. *Proc. 11th Int. Conf. on Atmospheric Electricity,* Guntersville, AL, NASA/CP-1999-209261, 715–718.

DeMott, C. A., and S. A. Rutledge, 1998: The vertical structure of TOGA COARE convection. Part I: Radar echo distributions. *J. Atmos. Sci.,* **55,** 2730–2747.

Dye, J. E., and Coauthors, 1986: Early electrification and precipitation development in a small, isolated Montana cumulonimbus. *J. Geophys. Res.,* **91,** 1231–1247.

——, W. P. Winn, J. J. Jones, and D. W. Breed, 1989: The electrification of New Mexico thunderstorms. 1. Relationship between precipitation development and the onset of electrification. *J. Geophys. Res.,* **94,** 8643–8656.

Hakkarinen, I. M., and R. F. Adler, 1988: Observations of convective precipitation at 92 and 183 GHz: Aircraft results. *Meteor. Atmos. Phys.,* **38,** 164–182.

Hall, T. J., and T. H. Vonder Harr, 1999: The diurnal cycle of west Pacific deep convection and its relation to the spatial and temporal variation of tropical MCSs. *J. Atmos. Sci.,* **56,** 3401–3415.

Heymsfield, G. M., I. J. Caylor, J. M. Shepherd, W. S. Olson, S. W. Bidwell, W. C. Boncyk, and S. Ameen, 1996: Structure of Florida thunderstorms using high-altitude aircraft radiometer and radar observations. *J. Appl. Meteor.,* **35,** 1736–1762.

Houze, R. A., 1993: *Cloud Dynamics.* Academic Press, 573 pp.

Iguchi, T., and R. Meneghini, 1994: Intercomparison of single-frequency methods for retrieving a vertical rain profile from airborne or spaceborne radar data. *J. Atmos. Oceanic Technol.,* **11,** 1507–1516.

Jorgensen, D. P., and M. A. LeMone, 1989: Mesoscale and convective-scale characteristics of oceanic convection. *J. Atmos. Sci.,* **46,** 621–640.

——, E. J. Zipser, and M. A. LeMone, 1985: Vertical motions in intense hurricanes. *J. Atmos. Sci.,* **42,** 839–856.

Kummerow, C., W. Barnes, T. Kozu, J. Shiue, and J. Simpson, 1998: The Tropical Rainfall Measuring Mission (TRMM) sensor package. *J. Atmos. Oceanic Technol.,* **15,** 809–817.

Lucas, C., E. J. Zipser, and M. A. LeMone, 1994: Vertical velocity in oceanic convection off tropical Australia. *J. Atmos. Sci.,* **51,** 3183–3193.

Maddox, R. A., 1980: An objective technique for separating macroscale and mesoscale features in meteorological data. *Mon. Wea. Rev.,* **108,** 1108–1121.

Mapes, B. E., and R. A. Houze Jr., 1993: Cloud clusters and super-clusters over the oceanic warm pool. *Mon. Wea. Rev.,* **121,** 1398–1415.

Mohr, K. I., and E. J. Zipser, 1996: Mesoscale convective systems defined by their 85-GHz ice scattering signature: Size and intensity comparison over tropical oceans and continents. *Mon. Wea. Rev.,* **124,** 2417–2437.

——, J. S. Famiglietti, and E. J. Zipser, 1999: The contribution to tropical rainfall with respect to convective system type, size, and intensity estimated from the 85-GHz ice-scattering signature. *J. Appl. Meteor.,* **38,** 596–606.

Mugnai, A., E. A. Smith, and G. J. Tripoli, 1993: Foundations for statistical–physical precipitation retrieval from passive microwave satellite measurements. Part II: Emission-source and generalized weighting-function properties of a time-dependent cloud-radiation model. *J. Appl. Meteor.,* **32,** 17–39.

Petersen, W. A., S. A. Rutledge, and R. E. Orville, 1996: Cloud-to-ground lightning observations from TOGA COARE: Selected results and lightning location algorithms. *Mon. Wea. Rev.,* **124,** 602–620.

Rickenbach, T. M., and S. A. Rutledge, 1998: Convection in TOGA COARE: Horizontal scale, morphology, and rainfall production. *J. Atmos. Sci.,* **55,** 2715–2729.

Riehl, H., and J. S. Malkus, 1958: On the heat balance in the equatorial trough zone. *Geophysica,* **6,** 503–538.

Smith, E. A., A. Mugnai, H. J. Cooper, G. J. Tripoli, and X. Xiang, 1992: Foundations for statistical–physical precipitation retrieval from passive microwave satellite measurements. Part I: Brightness-temperature properties of a time-dependent cloud-radiation model. *J. Appl. Meteor.,* **31,** 506–531.

Spencer, R. W., 1986: A satellite passive 37-GHz scattering-based method for measuring oceanic rain rates. *J. Climate Appl. Meteor.,* **25,** 754–766.

——, H. M. Goodman, and R. E. Hood, 1989: Precipitation retrieval over land and ocean with the SSM/I: Identification and characteristics of the scattering signal. *J. Atmos. Oceanic Technol.,* **6,** 254–273.

Takahashi, T., 1978: Electrical properties of oceanic tropical clouds at Ponape, Micronesia. *Mon. Wea. Rev.,* **106,** 1598–1612.

Vivekanandan, J., J. Turk, and V. N. Bringi, 1991: Ice water path estimation and characterization using passive microwave radiometry. *J. Appl. Meteor.,* **30,** 1407–1421.

Williams, E. R., R. Zhang, and J. Rydock, 1991: Mixed-phase microphysics and cloud electrification. *J. Atmos. Sci.,* **48,** 2195–2203.

——, S. A. Rutledge, S. G. Geotis, N. Renno, E. Rasmussen, and T. Rickenbach, 1992: A radar and electrical study of tropical "hot towers." *J. Atmos. Sci.,* **49,** 1386–1395.

Zipser, E. J., 1994: Deep cumulonimbus cloud systems in the Tropics with and without lightning. *Mon. Wea. Rev.,* **122,** 1837–1851.

——, and M. A. LeMone, 1980: Cumulonimbus and vertical velocity events in GATE. Part II: Synthesis and model core structure. *J. Atmos. Sci.,* **37,** 2458–2469.

——, and K. R. Lutz, 1994: The vertical profile of radar reflectivity of convective cells: A strong indicator of storm intensity and lightning probability? *Mon. Wea. Rev.,* **122,** 1751–1759.